Novel Rubredoxin Model Tetrathiolato Iron(II) and Cobalt(II) Complexes Containing Intramolecular Single and Double NH···S Hydrogen Bonds

Taka-aki Okamura, Satoshi Takamizawa, Norikazu Ueyama, and Akira Nakamura*

Department of Macromolecular Science, Graduate School of Science, Osaka University, Toyonaka, Osaka 560, Japan

Received May 30, 1997

Simple rubredoxin model complexes with *o*-(acylamino)benzenethiolato and 2,6-(diacylamino)benzenethiolato were synthesized and characterized by ^{1}H NMR, IR, and electrochemical properties. The structures of $(NEt_4)_2[Fe^{II}(S\text{-}o\text{-}t\text{-}BuCONHC_6H_4)_4]\cdot 2EtCN$ (**3a**), $(NEt_4)_2[Co^{II}(S\text{-}o\text{-}t\text{-}BuCONHC_6H_4)_4]\cdot 2EtCN$ (**3b**), and $(PPh_4)_2[Co^{II}\{S\text{-}2,6\text{-}(CF_3CONH)_2C_6H_3\}_4]\cdot Et_2O$ (**5b′**) were determined by X-ray analysis. The complexes have intramolecular single or double NH···S hydrogen bonds. The mean Fe−S and Co−S distances are significantly shorter than those of non-hydrogen-bonding complexes, $[M(SPh)_4]^{2-}$ (M = Fe(II), Co(II)), by 0.024 Å (**3a**), 0.032 Å (**3b**), and 0.029 Å (**5b′**), respectively. $(NMe_4)_2[Fe^{II}(S\text{-}o\text{-}CH_3CONHC_6H_4)_4]$ (**2a**) and $(NMe_4)_2[Fe^{II}\{S\text{-}2,6\text{-}(CH_3CONH)_2C_6H_3\}_4]$ (**6a**) have remarkably positive shifted Fe(III)/Fe(II) redox couples by the single and double NH···S hydrogen bond, respectively. The shifts are +0.25 for **2a** and +0.56 for **6a** from the redox potential of $[Fe^{II}(SPh)_4]^{2-}$, which indicate additivity of the effect of the NH···S hydrogen bond. The formation and the structure of a novel chelating amido(thiolato) complex $(PPh_4)_2[Co^{II}\{S\text{-}2,6\text{-}(CF_3CONH)_2C_6H_3\}_2(S\text{-}2\text{-}CF_3CONH\text{-}6\text{-}CF_3CONC_6H_3)]\cdot Et_2O$ (**9**) are also described.

Introduction

The biological importance of the NH···S hydrogen bond has been particularly notable for electron transfer metalloproteins, e.g. rubredoxins (1Fe),[1] ferredoxins ([2Fe-2S], [4Fe-4S]),[2] high-potential iron−sulfur proteins (HiPIP),[3] and blue copper proteins.[4,5] The presence of an NH···S hydrogen bond has been widely proposed by X-ray analysis,[1−7] Raman spectroscopy,[8−11] ENDOR (electron nuclear double resonance),[12,13] and NMR spectroscopic techniques[14] in various metalloproteins. The NH···S hydrogen bond is formed from sulfur on cysteine and an amide NH group on the main chain of peptide, and the bond is classified as single or double according to the number of amide NH interacting with one sulfur atom. Double NH···S hydrogen bonding has been observed in metalloproteins[3−5] and also in the model complex.[15,16]

The correlation between the redox potential and the NH···S hydrogen bond has been investigated for some complexes with [4Fe-4S] clusters, and the number and extent of NH···S hydrogen bonds have been considered to control the redox potential of active center.[17,18] We have already demonstrated the contribution of the NH···S hydrogen bond to the redox potential in ferredoxin and rubredoxin peptide model complexes.[15,19,20] Their exact structures have not been determined by X-ray analysis, since such peptide complexes are difficult to crystallize because of their flexibility or mobility. However, their properties are essentially important in biological regulation systems.

As communicated in a previous paper, we designed structurally unique rubredoxin model complexes with intraligand single NH···S hydrogen bonds and found mono(acylamino) substitution at the ortho position of benzenethiolato positively shifts the redox potential of Fe(II) thiolates.[21] In this paper, we report syntheses of complexes containing double NH···S hydrogen

(1) Watenpaugh, K. D.; Sieker, L. C.; Jensen, L. H. *J. Mol. Biol.* **1979**, *131*, 509.
(2) Tsukihara, T.; Fukuyama, K.; Nakamura, M.; Katsube, Y.; Kanaka, N.; Kakudo, M.; Hase, T.; Wada, K.; Matsubara, H. *J. Biochem.* **1981**, *90*, 1763.
(3) Adman, E.; Watenpaugh, K. D.; Jensen, L. H. *Proc. Natl. Acad. Sci. U.S.A.* **1975**, *72*, 4854−4855.
(4) Adman, E. T. *Adv. Protein Chem.* **1991**, *42*, 145−197.
(5) Baker, E. N. *J. Mol. Biol.* **1988**, *203*, 1071−1095.
(6) Kissinger, C. R.; Sieker, L. C.; Adman, E. T.; Jensen, L. H. *J. Mol. Biol.* **1991**, *219*, 693−715.
(7) Robbins, A. H.; McRee, D. E.; Williamson, M.; Collett, S. A.; Xuong, N. H.; Furey, W. F.; Wang, B. C.; Stout, C. D. *J. Mol. Biol.* **1991**, *221*, 1269−1293.
(8) Backes, G.; Mino, Y.; Loehr, T. M.; Meyer, T. E.; Cusanovich, M. A.; Sweeey, W. V.; Adman, E. T.; Sanders-Loehr, J. *J. Am. Chem. Soc.* **1991**, *113*, 2055−2064.
(9) Ainscough, E. W.; Bingham, A. G.; Brodie, A. M.; Ellis, W. R.; Gray, H. B.; Loehr, T. M.; Plowman, J. E.; Norris, G. E.; Baker, E. N. *Biochemistry* **1987**, *26*, 71−82.
(10) Han, J.; Adman, E. T.; Beppu, T.; Codd, R.; Freeman, H. C.; Huq, L.; Loehr, T. M.; Sanders-Loehr, J. *Biochemistry* **1991**, *30*, 10904−10913.
(11) Mino, Y.; Loehr, T. M.; Wada, K.; Matsubara, H.; Sanders-Loehr, J. *Biochemistry* **1987**, *26*, 8059−8065.
(12) Houseman, A. L. P.; Oh, B.; Kennedy, M. C.; Fan, C.; Werst, M. M.; Beinert, H.; Markley, J. L.; Hoffman, B. M. *Biochemistry* **1992**, *31*, 2073−2080.
(13) Fan, C.; Kennedy, M. C.; Beinert, H.; Hoffman, B. M. *J. Am. Chem. Soc.* **1992**, *114*, 374−375.
(14) Blake, P. R.; Park, J. B.; Adams, M. W. W.; Summers, M. F. *J. Am. Chem. Soc.* **1992**, *114*, 4931−4933.
(15) Sun, W.-Y.; Ueyama, N.; Nakamura, A. *Inorg. Chem.* **1991**, *30*, 4026−4031.
(16) Walters, M. A.; Dewan, J. C.; Min, C.; Pinto, S. *Inorg. Chem.* **1991**, *30*, 2656−2662.
(17) Carter, C. W., Jr. *J. Biol. Chem.* **1977**, *252*, 7802−7811.
(18) Sheridan, R. P.; Allen, L. C.; Carter, C. W. J. *J. Biol. Chem.* **1981**, *256*, 5052−5057.
(19) Nakamura, A.; Ueyama, N. *Adv. Inorg. Chem.* **1989**, *33*, 39−67.
(20) Ueyama, N.; Terakawa, T.; Nakata, M.; Nakamura, A. *J. Am. Chem. Soc.* **1983**, *105*, 7098−7101.
(21) Ueyama, N.; Okamura, T.; Nakamura, A. *J. Chem. Soc., Chem. Commun.* **1992**.

S0020-1669(97)00640-X CCC: $15.00
Published on Web 01/12/1998

bonds and discuss the functional differences between single and double NH···S hydrogen bonds in Fe(II) and related Co(II) complexes.

Experimental Section

All procedures were performed in an argon atmosphere using Schlenk techniques. All solvents were dried and distilled under argon before use.

2,2′-Dithiobis(*N*-phenyl-2,2-dimethylpropanamide), *N*-(4-mercaptophenyl)-2,2-dimethylpropanamide, (2,6-diaminophenyl) disulfide, and bis(2,6-(diacetylamino)phenyl) disulfide were prepared by the reported methods.[22−24] $(NEt_4)_2[MCl_4]$ (M = Fe, Co) was prepared by the literature procedure.[25] $(NEt_4)_2[Co(SC_6H_4)_4]$ and $(NEt_4)_2[Co(S\text{-}o\text{-}CH_3C_6H_4)_4]$ were synthesized by the same method reported for Ni(II) complexes.[26]

Bis[2-(triphenylacetylamino)phenyl)] Disulfide. To a tetrahydrofuran (THF) solution (10 mL) of triphenylacetic acid (2.0 g, 6.9 mmol) was added thionyl chloride (2 mL) with stirring, and the mixture was refluxed for 2 h. The solution was evaporated to dryness. The obtained acid chloride was dissolved in THF (5 mL) and then added dropwise to a THF solution (10 mL) of di(aminophenyl) disulfide (0.72 g, 2.9 mmol) and NEt_3 (0.8 mL, 5.8 mmol) in an ice bath. After stirring overnight, the solvent was removed under reduced pressure. The residue was extracted with ethyl acetate, washed with 2% HCl aq, sat. NaCl aq, 4% $NaHCO_3$ aq, and sat. NaCl aq successively, and dried over Na_2SO_4. After removal of the solvent, the oily product was recrystallized from ethyl acetate/diethyl ether to give white powder 1.5 g (67%). ^{1}H NMR (chloroform-d_1): δ 6.74 (d 2H), 6.80 (t 2H), 7.2−7.4 (m 32H), 8.57 (d 2H), 8.61 (s 2H). Anal. Calcd for $C_{52}H_{40}N_2O_2S_2$: C, 79.16; H, 5.11; N, 3.55. Found: C, 75.11; H, 4.94; N, 3.65. Mp: 212 °C. Mass (FAB): 789.2 (MH^+).

Bis[2,6-(trifluoroacetylamino)phenyl] Disulfide. To a THF solution (20 mL) of bis(2,6-diaminophenyl) disulfide (0.5 g, 1.8 mmol) was added trifluoroacetic anhydride (2.5 mL, 18 mmol) at 0 °C. The solution was stirred overnight at room temperature, 10 mL of water was added, and the resulting solution was concentrated to give an oily residue, which was dissolved in a mixture of ethyl acetate (200 mL) and water (50 mL). The organic layer was washed with 2% HCl aq, sat. NaCl aq, 4% $NaHCO_3$ aq, and sat. NaCl aq successively, dried over Na_2SO_4, and concentrated to dryness. The crude product was recrystallized from diethyl ether to give pale yellow crystals. Yield: 0.73 g (62%). ^{1}H NMR (chloroform-d_1): δ 7.64 (t 2H), 8.22 (d 4H), 8.60 (s 4H). Anal. Calcd for $C_{20}H_{10}N_4O_4F_{12}S_2$: C, 36.26; H, 1.52; N, 8.46. Found: C, 36.36; H, 1.73; N, 8.68.

$(NMe_4)_2[Fe^{II}(S\text{-}o\text{-}CF_3CONHC_6H_4)_4]\cdot Et_2O$ (1a). To an acetonitrile solution (5 mL) of $(S\text{-}o\text{-}CF_3CONHC_6H_4)_2$ (220 mg, 0.49 mmol) was added an acetonitrile solution (5 mL) of $(NMe_4)_2[Fe(SPh)_4]$ (130 mg, 0.20 mmol), and the resulting solution was stirred for 12 h. The reaction mixture was concentrated under reduced pressure. The obtained oily residue was recrystallized from acetonitrile/diethyl ether (1:10 v/v) and washed with diethyl ether to give pale yellow microcrystals. Yield: 210 mg (95%). Anal. Calcd for $C_{44}H_{54}N_6O_5F_{12}S_4Fe$: C, 45.60; H, 4.70; N, 7.25. Found: C, 45.36; H, 4.56; N, 7.32.

$(NMe_4)_2[Co^{II}(S\text{-}o\text{-}CF_3CONHC_6H_4)_4]\cdot Et_2O$ (1b). The titled compound was prepared from $(S\text{-}o\text{-}CF_3CONHC_6H_4)_2$ and $(NMe)_2[Co(SPh)_4]$ by a method analogous to that for **1a**. The crude product was recrystallized from acetonitrile/diethyl ether (1:10 v/v) to give yellow crystals. Yield: 85%. Anal. Calcd for $C_{44}H_{54}N_6O_5F_{12}S_4Co$: C, 45.48; H, 4.68; N, 7.23. Found: C, 44.81; H, 4.56; N, 7.38. The crystal solvent was easily removed under reduced pressure.

$(NMe_4)_2[Fe^{II}(S\text{-}o\text{-}CH_3CONHC_6H_4)_4]$ (2a). The complex was synthesized by a method similar to that described for **1a**. The crude oily product was washed with 1,2-dimethoxyethane (DME) to give brown powder. Unfortunately the product could not be crystallized from any solvent tried. Yield: 32%. Anal. Calcd for $C_{40}H_{56}N_6O_4S_4Fe$: C, 55.28; H, 6.50; N, 9.67. Found: C, 52.20; H, 6.65; N, 8.92. The result of elemental analysis did not show good agreement with the calculated value. The product was characterized, and its purity was confirmed by ^{1}H NMR spectra in acetonitrile-d_3.

$(NEt_4)_2[Fe^{II}(S\text{-}o\text{-}t\text{-}BuCONHC_6H_4)_4]\cdot 2EtCN$ (3a). A mixture of $(NEt_4)_2[FeCl_4]$ (230 mg, 0.50 mmol), 2,2′-dithiobis(*N*-phenyl-2,2-dimethylpropanamide) (500 mg, 1.2 mmol), and NEt_4BH_4 (170 mg, 1.2 mmol) was stirred in 1,2-dimethoxyethane (DME, 25 mL) for 3 days. Insoluble material was removed by filtration. The pale yellow solution obtained was concentrated under reduced pressure. The residual oil was crystallized form propionitrile/diethyl ether. The crude product was recrystallized from hot propionitrile, and extremely air-sensitive pale yellow octahedron-shaped crystals were obtained. Yield: 110 mg (20%). Anal. Calcd for $C_{66}H_{106}N_8O_4S_4Fe$: C, 62.93; H, 8.48; N, 8.90. Found: C, 62.68; H, 8.55; N, 8.91. This complex was also synthesized by the ligand exchange reaction described for **1a**.

$(NEt_4)_2[Co^{II}(S\text{-}o\text{-}t\text{-}BuCONHC_6H_4)_4]\cdot 2EtCN$ (3b). The complex was synthesized by the same method as described for **1a**. Green octahedron-shaped crystals were obtained in 91% yield. Anal. Calcd for $C_{66}H_{106}N_8O_4S_4Co$: C, 62.77; H, 8.46; N, 8.87. Found: C, 62.56; H, 8.46; N, 8.92. When recrystallization was performed from propionitrile/diethyl ether, prismatic crystals without propionitrile were obtained. Anal. Calcd for $C_{60}H_{96}N_6O_4S_4Co$: C, 62.52; H, 8.39; N, 7.29. Found: C, 62.24; H, 8.39; N, 7.36.

$(NEt_4)_2[Co^{II}(S\text{-}o\text{-}t\text{-}BuCOND C_6H_4)_4]$. The cobalt complex, **2**, was dissolved in deuterated methanol, CH_3OD. After stirring for several minutes, the solution was concentrated to dryness. The process was repeated three times. The resulting residue was dissolved in acetonitrile-d_3 for ^{1}H NMR measurement. The amide protons were deuterated to 70%.

$(NMe_4)_2[Fe^{II}(S\text{-}o\text{-}Ph_3CCONHC_6H_4)_4]$ (4a). A solution of $(NMe_4)_2[Fe(SPh)_4]$ (41 mg, 0.041 mmol) and $(S\text{-}o\text{-}Ph_3CCONHC_6H_4)_2$ (110 mg, 0.14 mmol) in a mixture of acetonitriole (5 mL) and THF (2 mL) was stirred overnight. The solvent was removed under reduced pressure. The residue was extracted with 3 mL of acetonitrile. The solution was concentrated to deposit precipitates, which were dissolved by heating and then left to stand in a refrigerator. The crystals was collected by filtration, washed twice with cold acetonitrile and diethyl ether, and dried *in vacuo*. Greenish yellow needles were obtained. Yield: 38 mg (33%). Anal. Calcd for $C_{112}H_{104}N_6O_4S_4Fe$: C, 75.48; H, 5.88; N, 4.72. Found: C, 74.93; H, 5.87; N, 4.74.

$(NMe_4)_2[Co^{II}(S\text{-}o\text{-}Ph_3CCONHC_6H_4)_4]$ (4b). The compound was synthesized by the same method described for **4a**. Light green needles were obtained in 34% yield. Anal. Calcd for $C_{112}H_{104}N_6O_4S_4Co$: C, 75.35; H, 5.87; N, 4.71. Found: C, 74.89; H, 5.78; N, 4.55.

$(NMe_4)_2[Fe^{II}\{S\text{-}2,6\text{-}(CF_3CONH)_2C_6H_3\}_4]\cdot 2CH_3CN$ (5a). To a solution (5 mL) of $(NMe_4)_2[Fe(SPh)_4]$ (39 mg, 0.060 mmol) in acetonitrile was added an acetonitrile solution (3 mL) of $\{S\text{-}2,6\text{-}(CF_3CONH)_2C_6H_3\}_2$ (100 mg, 0.15 mmol). After stirring for 6 h, insoluble materials were removed by filtration and the filtrate was concentrated under reduced pressure. The residue was recrystallized from acetonitrile/diethyl ether. Pale yellow prisms were deposited, washed with diethyl ether, and dried *in vacuo* to yield 79 mg (82%). Anal. Calcd for $C_{52}H_{50}N_{12}O_8F_{24}S_4Fe$: C, 38.77; H, 3.13; N, 10.43. Found: C, 38.65; H, 3.07; N, 10.09.

$(NMe_4)_2[Co^{II}\{S\text{-}2,6\text{-}(CF_3CONH)_2C_6H_3\}_4]$ (5b). The compound was prepared from $(NMe_4)_2[Co(SPh)_4]$ and $\{S\text{-}2,6\text{-}(CF_3CONH)_2C_6H_3\}_2$ by the method described for **5a**. Green thin needles were obtained in 48% yield. Anal. Calcd for $C_{48}H_{44}N_{10}O_8F_{24}S_4Co$: C, 37.63; H. 2.89; N, 8.72. Found: C, 37.98; H, 3.18; N, 9.00.

$(PPh_4)_2[Co^{II}\{S\text{-}2,6\text{-}(CF_3CONH)_2C_6H_3\}_4]$ (5b′). The compound was synthesized by the same method described for **5** using PPh_4^+ salts. Green plates were obtained by the recrystallization from acetonitrile/diethyl ether. Yield: 96%. Anal. Calcd for $C_{88}H_{60}N_8O_8F_{24}P_2S_4Co$: C, 51.24; H, 2.93; N, 5.43. Found: C, 52.41; H, 3.16; N, 5.66. This complex contains one molecule of diethyl ether as crystal solvent which was very easily removed.

(22) Ueyama, N.; Okamura, T.; Nakamura, A. *J. Am. Chem. Soc.* **1992**, *114*, 8129−8137.
(23) Ward, E. R.; Heard, D. D. *J. Chem. Soc.* **1965**, 1023−1028.
(24) Ueyama, N.; Okamura, T.; Yamada, Y.; Nakamura, A. *J. Org. Chem.* **1995**, *60*, 4893−4899.
(25) Gill, N. S.; Taylor, F. B. *Inorg. Synth.* **1967**, *9*, 136−142.
(26) Rosenfield, S. G.; Armstrong, W. H.; Mascharak, P. K. *Inorg. Chem.* **1986**, *25*, 3014−3018.

Table 1. Crystallographic Data for Iron(II) and Cobalt(II) Complexes

	3a	**3b**	**5b′**	**9**
empirical formula	$C_{66}H_{106}N_8O_4S_4Fe$	$C_{66}H_{106}N_8O_4S_4Co$	$C_{92}H_{70}N_8O_9F_{24}P_2S_4Co$	$C_{82}H_{64}N_6O_7F_{18}P_2S_3Co$
fw	1259.70	1262.79	2136.70	1804.47
cryst syst	tetragonal	tetragonal	triclinic	triclinic
a, Å	14.477(5)	14.475(8)	13.502(3)	13.782(5)
b, Å	14.477(5)	14.475(8)	28.031(5)	26.120(7)
c, Å	35.221(4)	35.14(1)	13.464(3)	13.756(4)
α, deg	90	90	90.62(2)	100.48(3)
β, deg	90	90	105.73(2)	119.64(2)
γ, deg	90	90	96.00(2)	94.33(3)
V, Å^3	7381(5)	7363(8)	4874(2)	4152(2)
Z	4	4	2	2
space group	$P4_12_12$	$P4_12_12$	$P\bar{1}$	$P\bar{1}$
μ, cm^{-1}	3.57	3.86	3.91	4.09
d_{calcd}, g cm^{-3}	1.133	1.139	1.456	1.443
$2\theta_{max}$, deg	50.1	60.1	55.1	55.1
scan type	*ω*	*ω*	*ω*	*ω*
no. of reflcns measd	total 3189	4932	unique 20 217	19 158
no. of obsd reflcns with $I > 3\sigma(I)$	1094	1925	9301	7796
R^a	0.077	0.077	0.072	0.079
$R_w{}^b$	0.076	0.089	0.083	0.083

^{a} $R = \sum||F_o| - |F_c||/\sum|F_o|$. ^{b} $R_w = [\sum w(|F_o| - |F_c|)^2/\sum w|F_o|^2]^{1/2}$; $w = 1/\sigma^2(|F_o|)$.

$(NMe_4)_2[Fe^{II}\{S\text{-}2,6\text{-}(CH_3CONH)_2C_6H_3\}_4]$ (6a). The compound was synthesized by the ligand exchange reaction of $(NMe_4)_2[Fe(SPh)_4]$ and $\{S\text{-}2,6\text{-}(CH_3CONH)_2C_6H_3\}_2$. The reaction mixture was concentrated followed by addition of diethyl ether. Pale yellow microcrystals were obtained in 93% yield. Anal. Calcd for $C_{48}H_{68}N_{10}O_8S_4Fe$: C, 52.54; H, 6.25; N, 12.77. Found: C, 50.82; H, 6.27; N, 12.40.

$(NMe_4)_2[Co^{II}\{S\text{-}2,6\text{-}(CH_3CONH)_2C_6H_3\}_4]$ (6b). This complex was synthesized by the method described for **6a** using $(NMe_4)_2[Co(SPh)_4]$. Yield: 74%. Anal. Calcd for $C_{48}H_{68}N_{10}O_8S_4Co$: C, 52.40 H, 6.23; N, 12.73. Found: C, 51.80; H, 6.18; N, 13.10.

$(NEt_4)_2[Fe^{II}(S\text{-}p\text{-}CH_3CONHC_6H_4)_4]$ (7a). A suspension of $(NEt_4)_2[Fe(SPh)_4]$ (49 mg, 0.065 mmol) and $(S\text{-}p\text{-}CH_3CONHC_6H_4)_2$ (52 mg, 0.16 mmol) in acetonitrile was stirred at room temperature. Immediately the mixture turned to a dark yellow clear solution. After addition of diethyl ether, the solution was stored at −20 °C to give greenish yellow microcrystals, which were recrystallized from acetonitrile/diethyl ether. Yield: 61%. Anal. Calcd for $C_{48}H_{72}N_6O_4S_4Fe$: C, 58.75; H, 7.40; N, 8.56. Found: C, 57.49; H, 7.58; N, 7.79.

$(NEt_4)_2[Co^{II}(S\text{-}p\text{-}t\text{-}BuCONHC_6H_4)_4]$ (8b). *N*-(4-Mercaptophenyl)-2,2′-dimethylpropanamide (210 mg, 1.0 mmol) and $(n\text{-}Bu)_3N$ (0.23 mL, 1.0 mmol) were dissolved in acetonitrile (3 mL). To this solution was added a solution of $(NEt_4)_2[CoCl_4]$ (96 mg, 0.2 mmol) in acetonitrile (3 mL). After the resulting solution had been stirred for 30 min, DME was added and green crystals precipitated. The crude product was recrystallized from hot propionitrile for several times to give green plates. Yield: 65 mg (27%). Anal. Calcd for $C_{66}H_{106}N_8O_4S_4Co$: C, 62.77; H, 8.46; N, 8.87. Found: C, 61.17; H, 9.01; N, 8.73. The value found does not give good agreement with the value calculated because of its extensive hygroscopicity.

$(PPh_4)_2[Co^{II}\{S\text{-}2,6\text{-}(CF_3CONH)_2C_6H_3\}_2(S\text{-}2\text{-}CF_3CONH\text{-}6\text{-}CF_3CONC_6H_3)]$ (9). An acetonitrile solution (3 mL) of **5b′** (125 mg, 0.061 mmol) was prepared under argon atmosphere. Air (2 mL) was bubbled through the solution at room temperature. After stirring for 6 h, the resulting dark green solution was concentrated under reduced pressure and the residue was recrystallized from acetonitrile/diethyl ether. Dark green plates were obtained. Yield: 72 mg (69%). Anal. Calcd for $C_{78}H_{54}N_6O_6P_2S_3F_{18}Co$: C, 54.14; H, 3.15; N, 4.86. Found: C, 53.93; H, 3.52; N, 4.80. This compound contains one molecule of diethyl ether which was easily removed without mother liquor.

Oxidation Reaction of 5b′. To a solution (0.3 mL, 0.25 mM) of **5b′** was added a solution (0.015 mL, 2.5 mM) of trimethylamine-*N*-oxide or $[FeCp_2]^+$. The reaction was followed by UV−visible spectral measurement in acetonitrile at room temperature. Air oxidation was performed in the same way using excess air.

Physical Measurements. UV−visible spectra were recorded in acetonitrile solution on a Jasco Ubest-30 spectrophotometer. ^{1}H NMR spectra were obtained on a Jeol GSX-400 spectrometer in acetonitrile-d_3 solution. IR spectra were taken on a Jasco DS-402G spectrometer. Samples were prepared as KBr pellets. Electrochemical measurements were carried out using a Yanaco P-1100 instrument in acetonitrile solution that contained 0.1 M tetra-*n*-butylammonium perchlorate as a supporting electrolyte. $E_{1/2}$ value, determined as $(E_{p,a} + E_{p,c})/2$, was referenced to the SCE electrode at room temperature and a value uncorrected with junction potential was obtained.

X-ray Structure and Determination. Suitable crystals of $(NEt_4)_2[Fe^{II}(S\text{-}o\text{-}t\text{-}BuCONHC_6H_4)_4]\cdot 2EtCN$ (**3a**), $(NEt_4)_2[Co^{II}(S\text{-}o\text{-}t\text{-}BuCONHC_6H_4)_4]\cdot 2EtCN$ (**3b**), $(PPh_4)_2[Co\{S\text{-}2,6\text{-}(CF_3CONH)_2C_6H_3\}_4]$ (**5b′**), and $(PPh_4)_2[Co\{S\text{-}2,6\text{-}(CF_3CONH)_2C_6H_3\}_2(S\text{-}2\text{-}CF_3CONH\text{-}6\text{-}CF_3CONC_6H_3)]\cdot Et_2O$ (**9**) were sealed in glass capillaries under an argon atmosphere. X-ray measurements of each were made at 23 °C on a Rigaku AFC5R diffractometer with graphite-monochromated Mo Kα radiation (0.710 69 Å). Unit cell dimensions were refined with 25 reflections. The basic crystallographic parameters for **3a**, **3b**, **5b′**, and **9** are listed in Table 1. Three standard reflections were chosen and monitored with every 100 reflections and did not show any significant change. An empirical absorption correction based on azimuthal scans of several reflections was applied. The structures were solved by direct methods using the TEXSAN crystallographic software package of the Molecular Structure Corp. (The Woodlands, TX).

In the case of **3a** and **3b**, the iron and cobalt atoms occupy the C_2 symmetrical special positions (*x*, *x*, 0). Positions for *t*-Bu groups and ethyl groups of NEt_4^+ were disordered. The refined multiplicity for the major positions are 0.702 (C81A−C83A in **1**), 0.634 (C84A−C86A in **1**), 0.775 (C81A−C83A in **2**), 0.625 (C84A−C86A in **2**), and 0.575 (C33A−C37A in **2**). The non-hydrogen atoms except C81B−C86B were refined anisotropically.

In the case of **5b′**, fluorine atoms of six CF_3 groups were found at disordered positions, which were refined isotropically. The refined multiplicities for the major positions are 0.674 (F4A−F6A), 0.535 (F10A−F12A), 0.729 (F13A−F15A), 0.652 (F16A−F18A), 0.569 (F19A−F21A), and 0.660 (F22A−F24A). The other non-hydrogen atoms were refined anisotropically.

In the case of **9**, fluorine atoms of four CF_3 groups were found at disordered positions. The refined multiplicities for the major positions are 0.659 (F1A−F3A), 0.848 (F10A−F12A), 0.572 (F13A−F15A), and 0.639 (F16A−F18A). The other non-hydrogen atoms except fluorines were refined anisotropically.

All hydrogen atoms were placed on the calculated positions. The final refinement was carried out using full-matrix least-squares techniques with non-hydrogen atoms. The final difference Fourier map showed no significant features. Atom scattering factors and dispersion

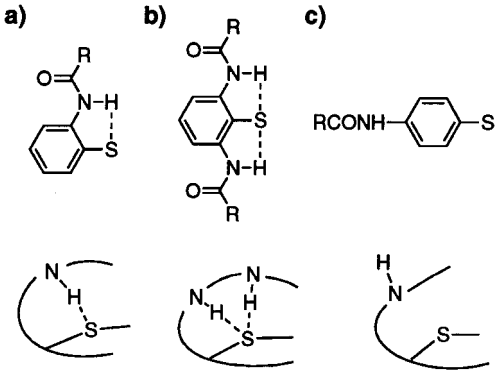

Figure 1. Schematic drawings of model ligands and the corresponding intramolecular interaction in peptide: (a) S-*o*-$RCONHC_6H_4$ (single NH···S hydrogen bond), (b) S-*2,6*-$(RCONH)_2C_6H_3$ (double NH···S hydrogen bond), and (c) S-*p*-$RCONHC_6H_4$ (without NH···S hydrogen bond).

corrections were taken from the *International Tables for X-ray Crystallography*.[27]

Results

Synthesis. We have designed two types of ligands with single or double NH···S hydrogen bond as models of peptides shown Figure 1. A ligand without NH···S hydrogen bond was also synthesized to check the inductive effect of amide group. Novel mononuclear iron(II) tetrathiolato anions were synthesized quantitatively by the redox-driven ligand exchange reaction using diaryl disulfide shown below.

$$(NMe_4)_2[Fe^{II}(SPh)_4] + 2ArS{-}SAr \xrightarrow[CH_3CN]{} (NMe_4)_2[Fe^{II}(SAr)_4] + 2PhS{-}SPh$$

The reaction was controlled by the difference of reduction potential of the disulfide as described in the corresponding copper(I) thiolate complex.[28] The reduction potentials of {S-2,6-$(CF_3CONH)_2C_6H_3$}$_2$ and (S-*o*-$CF_3CONHC_6H_4)_2$ were observed at −0.75 and −1.15 V (vs SCE), respectively, which are more positive than that (−1.92 V) of diphenyl disulfide. These results suggest NH···S hydrogen bonds stabilize the anionic ArS^- state. For a *para*-substituted ligand, (S-*p*-$CH_3CONHC_6H_4)_2$, we used this method to detect incomplete exchange. In the successful cases, low solubility of the product probably contributed to the ease of isolation. Similar syntheses have been reported for other related compounds with a molybdenum ion or a [4Fe-4S] cluster.[22,29,30]

Crystal Structures of $(NEt_4)_2[Fe^{II}$(S-*o*-*t*-BuCONHC$_6$H$_4)_4]$·2EtCN (3a), $(NEt_4)_2[Co^{II}$(S-*o*-*t*-BuCONHC$_6$H$_4)_4]$·2EtCN (3b), $(PPh_4)_2[Co^{II}${S-2,6-$(CF_3CONH)_2C_6H_3$}$_4]$ (5b′), and $(PPh_4)_2$-$[Co^{II}${S-2,6-$(CF_3CONH)_2C_6H_3$}$_2$(S-2-CF_3CONH-6-CF_3-$CONC_6H_3)]$ (9). Two complexes, **3a** and **3b**, crystallized in isomorphous packing with $P4_12_12$ space group. ORTEP views of **3a** and **3b** are shown in Figures 2 and 3, respectively. Selected bond distances and bond angles for the both complexes

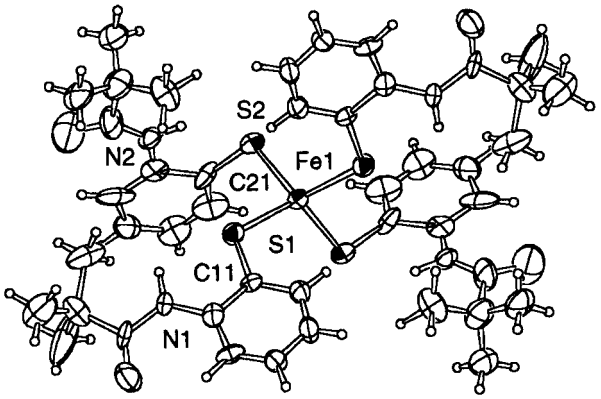

Figure 2. Perspective view of the anion part of $(NEt_4)_2[Fe^{II}$(S-*o*-*t*-$BuCONHC_6H_4)_4]$·2EtCN (**3a**).

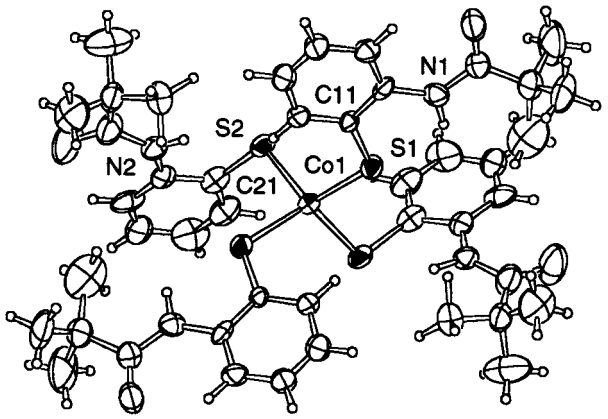

Figure 3. (a) Perspective view of the anion part of $(NEt_4)_2[Co^{II}$(S-*o*-*t*-$BuCONHC_6H_4)_4]$·2EtCN (**3b**). (b) Schematic drawing of **3b** where acylamino groups are omitted.

Table 2. Selected Bond Distances (Å) and Angles (deg) of $[M(SAr)_4]^{2-}$ (M = Fe(II), Co(II))

	3a	3b	5b′	9
M−S(1)	2.322(6)	2.288(4)	2.298(2)	2.331(2)
−S(2)	2.336(6)	2.304(3)	2.280(2)	2.327(2)
−S(3)[a]	2.322(6)	2.288(4)	2.303(2)	2.263(3)
−S(4)[a]	2.336(6)	2.304(3)	2.314(2)	−
mean	2.329	2.296	2.299	
M−N	−	−	−	2.049(5)
M−S(1)−C(11)	113.3(6)	113.5(4)	109.5(2)	103.8(2)
−S(2)−C(21)	107.0(7)	105.8(4)	113.7(2)	108.7(3)
−S(3)−C(31)	113.3(6)	113.5(4)	105.6(3)	94.9(3)
−S(4)−C(41)	107.0(7)	105.8(4)	112.5(2)	−
mean	110.2	109.7	110.3	
−N(6)−C(36)	−	−	−	112.7(5)
S(1)−M−S(2)	97.6(2)	112.1(1)	100.52(7)	99.32(8)
−S(3)	119.6(3)	123.7(2)	100.11(7)	120.5(1)
−S(4)	114.9(2)	97.1(1)	117.96(9)	−
S(2)−M−S(3)	114.9(2)	97.1(1)	112.44(9)	108.55(9)
−S(4)	113.3(3)	115.9(2)	119.03(8)	−
S(3)−M−S(4)	97.6(2)	112.1(1)	105.41(8)	−
N(6)−M−S(1)	−	−	−	108.3(2)
−S(2)	−	−	−	134.7(2)
−S(3)	−	−	−	87.6(2)

[a] For **3a** and **3b**, S(3) and S(4) indicate S(1*) and S(2*), respectively.

are listed in Table 2. Each molecule has a crystallographical C_2 axis which bisects the S−M−S (M = Fe, Co) angle. Their geometry is approximate S_4 symmetry. The S−M−S angles are bisected by the S_4 axis. The angles S(1)−M−S(3) and S(2)−M−S(4) are large (119.6, 113.3, 123.7, 115.9°) and form

(27) Cromer, D. T. *International Tables for X-ray Crystallography*; The Kynoch Press: Birmingham, England, 1974; Vol. IV, Table 2.2A.
(28) Okamura, T.; Ueyama, N.; Nakamura, A.; Ainscough, E. W.; Brodie, A. W.; Waters, J. W. *J. Chem. Soc., Chem. Commun.* **1993**, 1658−1659.
(29) Ueyama, N.; Yamada, Y.; Okamura, T.; Kimura, S.; Nakamura, A. *Inorg. Chem.* **1996**, *35*, 6473−6484.
(30) Que, L., Jr.; Bobrik, M. A.; Ibers, J. A.; Holm, R. H. *J. Am. Chem. Soc.* **1974**, *96*, 4168−4177.

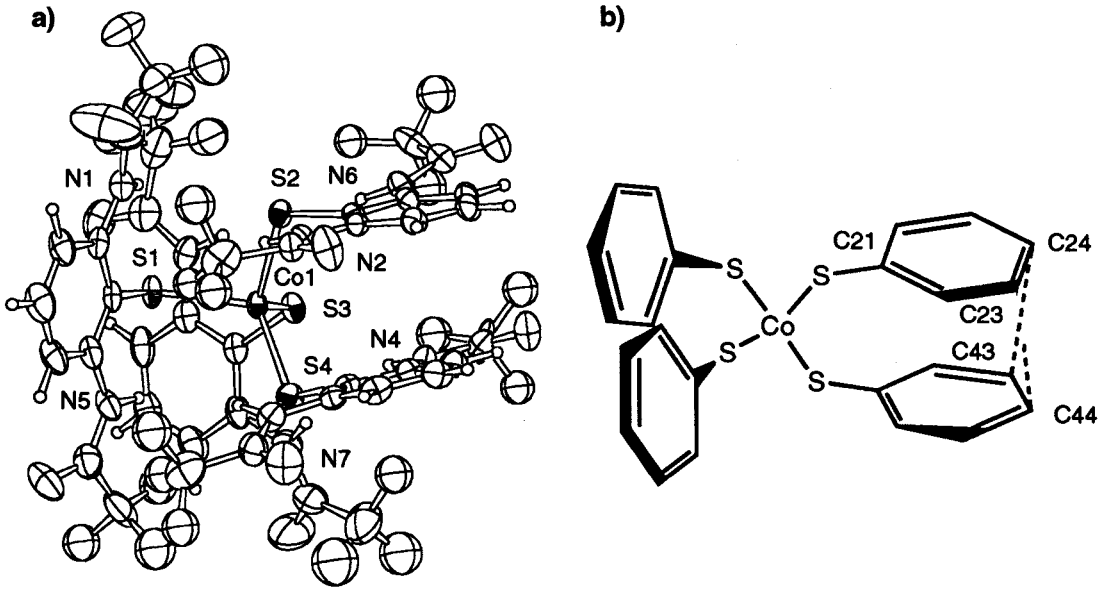

Figure 4. Perspective view of the anion part of $(PPh_4)_2[Co\{S\text{-}2,6\text{-}(CF_3CONH)_2C_6H_3\}_4]\cdot Et_2O$ (**5b′**).

Table 3. Intramolecular NH···S Contacts in the Crystal

	intraligand				interligand	
3a	N1···S1	2.92(2)	N2···S2	2.94(2)	–	
3b	N1···S1	2.89(1)	N2···S2	2.94(1)	–	
5b′	N1···S1	3.013(6)	N2···S2	2.911(6)	N1···S2	3.485(6)
	N3···S3	2.900(6)	N4···S4	3.018(6)	N3···S1	3.366(7)
	N5···S1	2.912(8)	N6···S2	2.947(7)	N5···S4	3.907(6)
	N7···S3	2.983(7)	N8···S4	2.938(7)	N7···S4	3.722(7)
9	N1···S1	2.940(8)	N2···S2	2.940(8)	N1···S3	3.901(6)
	N3···S3	2.917(8)	N4···S1	2.938(8)	N2···S3	3.417(6)
	N5···S2	2.931(9)			N4···S2	3.632(7)

a compressed MS_4 core as described in the literature.[31,32] The amide groups are approximately coplanar to the benzene ring with C(11)−C(12)−N(1)−C(17) dihedral angles of 167(2)° for **3a** and 172(1)° for **3b** and C(21)−C(22)−N(2)−C(27) angles of 169(2)° for **3a** and 164(1)° for **3b**, which are preferable to spread the π-conjugated system. The amide NH groups are directed to form intraligand NH···S hydrogen bonds of which N···S distances are 2.89−2.94 Å (Table 3).

Compounds **5b′** and **9** crystallized in space group $P\bar{1}$ with two nearly equal axes, *a* and *b*. The molecule packing and the anion shape for **5b′** resemble those for **9**. ORTEP views of **5b′** and **9** are shown in Figures 4 and 5, respectively. Most of the known tetra(arenethiolato) complexes with the same coordination geometry have axial-symmetrical structure, i.e. D_{2d} and S_4 conformers. The $Co(SC)_4$ core in **5b′** is remarkably distorted from D_{2d} and S_4 symmetry due to steric congestion of bulky CF_3CONH groups at 2,6-positions and short Co−S bonds. The two benzene rings of **5b′** show intramolecular stacking with C23···C44 = 3.35 Å, C24···C43 = 3.40 Å. At the corresponding position of **9**, the benzene rings are replaced by one S(thiolato), N(deprotonated amide)-chelate ligand which is preferable to avoid steric congestion. In the complex **5b′**, eight intraligand NH···S hydrogen bonds were found with N···S distances of 2.900−3.018 Å. Interligand NH···S contacts were found in **5b′** with short N···S distances below 4 Å as shown in Table 3.

Comparison with the corresponding nonsubstituted benzenethiolate complexes shows relatively short M−S bonds in **3a**, **3b**, and **5b′**, though the deviation is large. Such a tendency has been found in the previously reported analogous Cu(I) and Mo(V) complexes having intraligand NH···S hydrogen bonds.[22,28] The Fe−S bond length (mean 2.329(8) Å) of **3a** is shorter than that of $(PPh_4)_2[Fe^{II}(SC_6H_5)_4]$ (mean 2.353(9) Å)[33] by 0.024 Å. The Co−S bond length (mean 2.296(9) Å) of **3b** is shorter than that of $(PPh_4)_2[Co^{II}(SC_6H_5)_4]$ (mean 2.328(11) Å) by 0.032 Å. Relations between the M−S bond and the M−S−C angle have been reported for some benzenethiolate complexes.[34,35] Because the mean M−S−C angles of **3a**, **3b**, and **5b′** are similar to that (mean 109.9° for Co^{II}, 110.9° for Fe^{II}) of $[M(SPh)_4]^{2-}$ (M = Fe^{II} or Co^{II}),[33,35] the contribution of the M−S−C angle is now considered negligible in this case. The relationship between

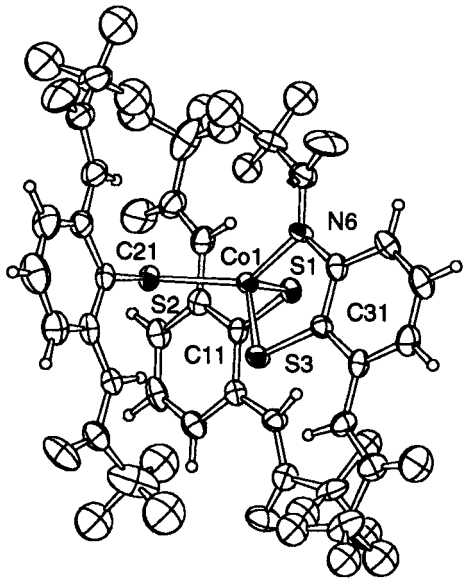

Figure 5. Perspective view of the anion part of $(PPh_4)_2[Co\{S\text{-}2,6\text{-}(CF_3CONH)_2C_6H_3\}_2(S\text{-}2\text{-}CF_3CONH\text{-}6\text{-}CF_3CONC_6H_3)]\cdot Et_2O$ (**9**).

(31) Maelia, L. E.; Millar, M.; Koch, S. A. *Inorg. Chem.* **1992**, *31*, 4594−4600.
(32) Silver, A.; Koch, S. A.; Millar, M. *Inorg. Chim. Acta* **1993**, *205*, 9−14.
(33) Coucouvanis, D.; Swenson, D.; Baenziger, N. C.; Murphy, C.; Holah, D. G.; Sfarnas, N.; Simopoulos, A.; Kostikas, A. *J. Am. Chem. Soc.* **1981**, *103*, 3350−3362.
(34) Ueyama, N.; Sugawara, T.; Sasaki, K.; Nakamura, A.; Yamashita, S.; Wakatsuki, Y.; Yamazaki, H.; Yasuoka, N. *Inorg. Chem.* **1988**, 741.
(35) Swenson, D.; Baenziger, N. C.; Coucouvanis, D. *J. Am. Chem. Soc.* **1978**, *100*, 1932−1934.

Table 4. Isotropic Shifts[a] of $(NEt_4)_2[M(SAr)_4]$ (M = Fe^{II}, Co^{II}) in Acetonitrile-d_3 at 30 °C

	ortho			meta		para	
	H	NH	CH_3	H		H	NH
$[Fe^{II}(S\text{-}o\text{-}CF_3CONHC_6H_4)_4]^{2-}$ [b]	−30.5	−7	−	21.9	16.1	−33.8	−
$[Co^{II}(S\text{-}o\text{-}CF_3CONHC_6H_4)_4]^{2-}$ [b]	−57.6	−6.4	−	19.6	11.9	−37.8	−
$[Fe^{II}(S\text{-}o\text{-}CH_3CONHC_6H_4)_4]^{2-}$ [b]	−28.2	−5	−	17.3	20.9	−32.5	−
$[Fe^{II}(S\text{-}o\text{-}t\text{-}BuCONHC_6H_4)_4]^{2-}$ [b]	−31.6	−15.0	−	21.4	15.9	−32.0	−
$[Co^{II}(S\text{-}o\text{-}t\text{-}BuCONHC_6H_4)_4]^{2-}$ [b]	−57.1	−12.9	−	20.1	10.9	−34.2	−
$[Fe^{II}(S\text{-}o\text{-}Ph_3CCONHC_6H_4)_4]^{2-}$ [b,f]	*e*	−13.8	−	22.2	18.6	−30.2	−
$[Co^{II}(S\text{-}o\text{-}Ph_3CCONHC_6H_4)_4]^{2-}$ [b,f]	56.2	−12.6	−	20.4	10.9	−30.4	−
$[Fe^{II}\{S\text{-}2,6\text{-}(CF_3CONH)_2C_6H_3\}_4]^{2-}$ [b]	−	+0.2	−	18.1		−40.1	−
$[Co^{II}\{S\text{-}2,6\text{-}(CF_3CONH)_2C_6H_3\}_4]^{2-}$ [b]	−	0.0	−	24.6		−47.0	−
$[Fe^{II}\{S\text{-}2,6\text{-}(CH_3CONH)_2C_6H_3\}_4]^{2-}$ [b]	−	2.6	−	19.0		−37.3	−
$[Co^{II}\{S\text{-}2,6\text{-}(CH_3CONH)_2C_6H_3\}_4]^{2-}$ [b]	−	2.0	−	30.1		−31.1	−
$[Fe^{II}(S\text{-}p\text{-}CH_3CONHC_6H_4)_4]^{2-}$ [c]	−24.1	−	−	15.7		−	3.1
$[Co^{II}(S\text{-}p\text{-}t\text{-}BuCONHC_6H_4)_4]^{2-}$ [c]	−39.4	−	−	10.2		−	5.3
$[Fe^{II}(S\text{-}o\text{-}CH_3C_6H_4)_4]^{2-}$ [c]	−69.6	−	24.5	19.6	8.4	−31.8	−
$[Fe^{II}(S\text{-}C_6H_5)_4]^{2-}$ [c,d]	−24.1	−	−	15.1		−30.7	−
$[Co^{II}(S\text{-}C_6H_5)_4]^{2-}$ [c]	−39.2	−	−	9.51		−30.7	−

[a] $(\Delta H/H_0)^{iso} = (\Delta H/H_0)^{obsd} - (\Delta H/H_0)^{dia}$ referred to [b]the disulfide of the ligand and [c]the corresponding thiol. [d] Value from ref 38. [e] Unobserved (broad signal). [f] Major peaks.

Fe−S distance and electron-donating capacity has been described.[31] In this case, the inductive effect of acylamino groups in the complexes **3a** and **3b** is negligible. Furthermore in the complex **5b′**, the weakly electron-withdrawing CF_3CONH group does not shorten the Co−S bond according to this effect. Thus another factor, e.g. the NH···S hydrogen bond, must be taken to account for this observation. The Co−S bond length (mean 2.299 Å) in **5b′** with double NH···S hydrogen bonds is near to that of **3b** with single NH···S hydrogen bonds. In the case of the other known hydrogen-bonding complexes, the average Co−S bond length of $[(C_6H_{11})_2NH_2]_2[Co(SC_6H_5)_4]$ and that of $[(CH_3NCH_2CONH_2][Co(SC_6H_5)_4]\cdot 0.5CH_3CN$ are 2.308 and 2.302(1) Å, respectively. The short Co−S bonds have been considered to be caused by the stabilization of metal−sulfur π-type antibonding orbital by interligand NH···S hydrogen bonds.

Complex **9** has two long Co−S bonds (mean 2.329 Å), one short Co−S bond (2.263(3) Å), and one Co−N bond (2.049 Å). In the monodentate ligand, the benzene ring is perpendicular to C−S−Co plane that reduces of the pπ (benzene ring)−pπ (S) overlap. Reduction of the pπ−pπ overlap thus decreases the M−S π-bond character.

IR Spectra. The IR spectra of **3b** in the solid state show low-wavenumber-shifted NH stretching (3281 cm^{-1}) and free carbonyl stretching (1667 cm^{-1}) compared with free ν(NH) (3397 cm^{-1}) and ν(C═O) (1688 cm^{-1}) of $(S\text{-}o\text{-}t\text{-}BuCONHC_6H_4)_2$ in a dilute CH_2Cl_2 solution. The results strongly suggest the presence of NH···S hydrogen bonds.[22,28,29] Lack of NH···O═C interaction was found in the complex, which is consistent with its solid state structure.

In the double NH···S hydrogen-bonded complex, $(PPh_4)_2[Co\{S\text{-}2,6\text{-}(CF_3CONH)_2C_6H_3\}_4]$ (**5b′**), the presence of intramolecular hydrogen bonds was established by IR spectroscopy. Only hydrogen-bonded amide stretchings were observed at 3256 cm^{-1} for ν(NH) and 1720 cm^{-1} for ν(C═O). The differences from ν(NH) and ν(C═O) of $\{S\text{-}2,6\text{-}(CF_3CONH)_2C_6H_3\}_2$ in CH_2Cl_2 are −114 and −27 cm^{-1}, respectively. The spectral pattern of $(PPh_4)_2[Co\{S\text{-}2,6\text{-}(CF_3CONH)_2C_6H_3\}_2(S\text{-}2\text{-}CF_3CONH\text{-}6\text{-}CF_3CONC_6H_3)]$ (**9**) in the amide stretching region resembles that of **5b′** except for the appearance of a new stretching at 1633 cm^{-1} which is assigned to ν(C═O) for the (S,N)-chelated ligand. The C═O bond is considered weakened by the coordination of Co^{2+} ion to the deprotonated amide N, although the C═O length (1.22(1) Å) by X-ray analysis does not reflect the effect.

UV−Visible Spectra. The iron complex **3a** indicates a very broad d−d transition at ca. 500−600 nm.[33] The absorption of **3a** in UV region is considered to be due to phenyl groups which is similar to that of **3b**. The cobalt complex **3b** shows an intense sulfur-to-cobalt charge transfer (CT) band at 420 nm (4600 M^{-1} cm^{-1}) and $^4A_2 \rightarrow {}^4T_1(P)$ transition at 687 nm (1000 M^{-1} cm^{-1}) in tetrahedral geometry.[33] The reported spectrum of $[Co(SC_6H_5)_4]^{2-}$ shows similar CT and d−d transitions at 420 and 690 nm, respectively.[35] The similar d−d transition is ascribed to similar ligand field around Co(II) in solution. The lack of significant difference between CT bands of **3b** and $[Co(SPh)_4]^{2-}$ [35] suggests almost negligible influence of NH···S hydrogen bond to the CT transitions. The reported interligand NH···S hydrogen bonded complexes, $[(C_6H_{11})_2NH_2]_2[Co(SC_6H_5)_4]$[36] and $[(CH_3)_3NCH_2CONH_2]_2[Co(SC_6H_5)_4]\cdot 0.5CH_3CN$,[16] also indicate a similar CT band in the solid state.

The other cobalt complexes described here show an absorption maximum at ca. 420 nm except for $(NMe_4)_2[Co^{II}(S\text{-}o\text{-}Ph_3CCONHC_6H_4)_4]$ which exhibits an absorption maximum at 443 nm (ϵ 4000). Because the electronic inductive effect of Ph_3C is similar to that of *t*-Bu from electrochemical results summarized in Table 5 and described in the results of electrochemical properties, other effects have to be considered. A phenyl (π) to sulfur (π) interaction is one of the most probable effects. In the rubredoxin peptide-model complexes having phenyl rings in the neighborhood of coordinated sulfur, a significant contribution of phenyl (pπ)−S(pπ) interaction to S → Fe(II) charge transfer (LMCT) absorption was reported.[37] In our case, π electrons on the phenyl ring must influence the electronic state on coordinated sulfur. If π electrons on the phenyl ring increase electron density on sulfur, the energy level of filled pπ orbitals on S^- is considered to rise and then results in appearance of a red-shifted LMCT absorption maximum as indicated above.

^{1}H NMR Spectra. Figure 6 shows the ^{1}H NMR spectra of $(NEt_4)_2[Fe^{II}(S\text{-}o\text{-}t\text{-}BuCONHC_6H_4)_4]$ (**3a**), $(NEt_4)_2[Co^{II}(S\text{-}o\text{-}t\text{-}BuCONHC_6H_4)_4]$ (**3b**), $(NEt_4)_2[Co^{II}(S\text{-}o\text{-}t\text{-}BuCONDC_6H_4)_4]$, and $(NEt_4)_2[Co^{II}(S\text{-}p\text{-}t\text{-}BuCONHC_6H_4)_4]$ (**8b**) in acetonitrile-

(36) Chung, W. P.; Dewan, J. C.; Walters, M. A. *J. Am. Chem. Soc.* **1991**, *113*, 525−530.
(37) Sun, W.-Y.; Ueyama, N.; Nakamura, A. *Inorg. Chem.* **1993**, *32*, 1095−1100.

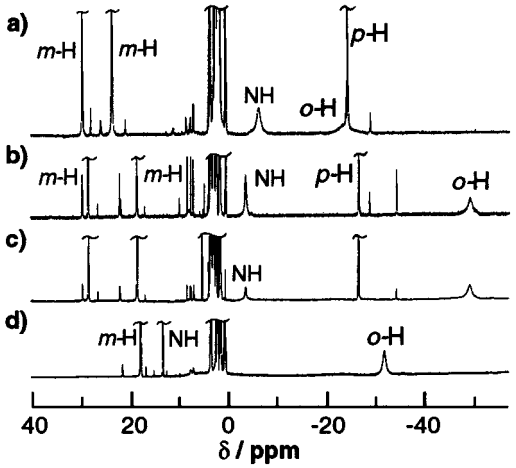

Figure 6. ^{1}H NMR spectra of (a) $(NEt_4)_2[Fe^{II}(S\text{-}o\text{-}t\text{-}BuCONHC_6H_4)_4]$, (b) $(NEt_4)_2[Co^{II}(S\text{-}o\text{-}t\text{-}BuCONHC_6H_4)_4]$, (c) $(NEt_4)_2[Co^{II}(S\text{-}o\text{-}t\text{-}BuCONDC_6H_4)_4]$ ((70% deuterated), and (d) $(NEt_4)_2[Co^{II}(S\text{-}p\text{-}t\text{-}BuCONHC_6H_4)_4]$ in acetonitrile-d_3.

d_3. The benzene ring protons were assigned according to the reported assignment.[38] The assignment of NH protons was performed with selective NH deuteration in methanol-d_1. In both cases of the Fe(II) and the Co(II) complexes, the ortho or para protons were observed at upfield. On the contrary, the protons at the meta position were observed at downfield. The broad NH signals of **3a** and **3b** appear at −6.7 and −4.6 ppm, respectively. On the other hand, **8b** exhibits a sharp NH signal at 13.2 ppm.

The isotropic shifts of ligand protons for some related complexes are listed in Table 4. The isotropic shifts were calculated from the relation $(\Delta H/H_0)^{iso} = (\Delta H/H_0)^{obsd} - (\Delta H/H_0)^{dia}$, where $(\Delta H/H_0)^{dia}$ (diamagnetic reference shifts) were taken as those of the free thiols or disulfides in acetonitrile. The *o*- and *p*-ring protons exhibit upfield shifts. On the other hand, the *m*-ring protons, *o*-methyl, and *p*-amide protons show downfield shifts. The alternate signs of the ring proton shifts have been interpreted by valence bond structure with delocalization in phenyl π orbitals.[39−41] The *o*-methyl proton signal has been explained by the hyperconjugative process.[39]

Interestingly, the *o*-amide NH signal was observed upfield shifted in the single-hydrogen-bonded complex. Although the π-conjugation causes downfield shift for *o*-amide proton as observed for *o*-methyl and *p*-amide protons, a different kind of magnetic effect must be considered.

The temperature dependence for ^{1}H NMR spectra of $(NMe_4)_2[Fe^{II}\{S\text{-}2,6\text{-}(CF_3CONH)_2C_6H_3\}_4]$ (**5a**) and $(NMe_4)_2[Co^{II}\{S\text{-}2,6\text{-}(CF_3CONH)_2C_6H_3\}_4]$ (**5b**) is shown in Figure 7. These complexes exhibit a very broad proton signal at 30 °C. The behavior of temperature dependence was different between the iron(II) and the cobalt(II) complexes. In the case of **5a**, the broad *m*- and *p*-H signals become sharp one on cooling. In contrast to the *p*-H signal of **5a**, the *p*-H signal of the cobalt complex, **5b**, exhibits two sharp peaks in 3:1 ratio at −30 °C. The broadening of the signals at room temperature is considered to be caused by two factors. One is a restricted or slow

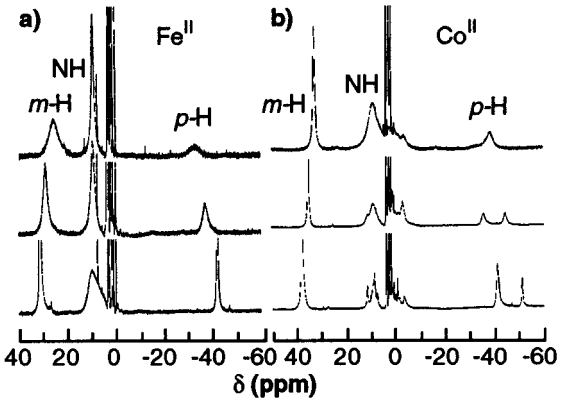

Figure 7. ^{1}H NMR spectra of (a) $(NMe_4)_2[Fe\{S\text{-}2,6\text{-}(CF_3CONH)_2C_6H_3\}_4]$ (**5a**) and (b) $(NMe_4)_2[Co\{S\text{-}2,6\text{-}(CF_3CONH)_2C_6H_3\}_4]$ (**5b**) in acetonitrile at 30 °C (top), 0 °C (middle), and −30 °C (bottom).

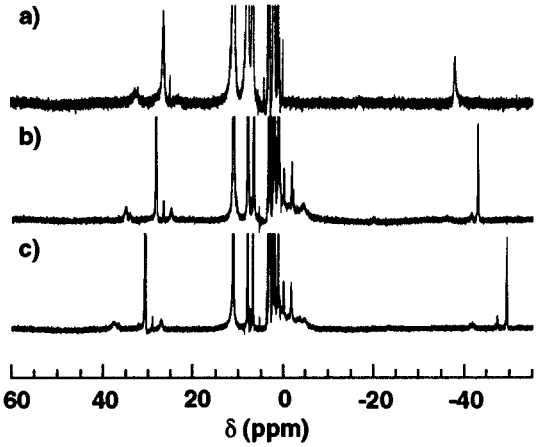

Figure 8. ^{1}H NMR spectra of a mixture of $(NMe_4)_2[Co\{S\text{-}2,6\text{-}(CF_3CONH)_2C_6H_3\}_4]$ and $(NMe_4)[S\text{-}2,6\text{-}(CF_3CONH)_2C_6H_3]$ (1:8 molar ratio) in acetonitrile-d_3 at (a) 30, (b) 0, and (c) −30 °C.

conformational change, and the other is dissociation of the ligand. Because the Co−S distance (mean 2.296 Å) of **5b** is shorter than the Fe−S distance (mean 2.329 Å) of **5a** as described above, the CoS_4 core has more steric crowding compared with the FeS_4 core.

The effect caused by the addition of excess of the thiolate ligand reveals that the predominant factor is the dissociation. In the case of the cobalt complex **5b**, the dissociation equilibrium is expressed by the equations shown below.

$$2[Co(SAr)_4]^{2-} \rightleftharpoons [Co_2(SAr)_6]^{2-} + 2SAr^-$$

and/or

$$[Co(SAr)_4]^{2-} + nCH_3CN \rightleftharpoons [Co\,(SAr)_{4-n}(CH_3CN)_n]^{2-} + nSAr^-$$

In this equation, the addition of ligands SAr^- increases the population of the monomeric complex $[Co(SAr)_4]^{2-}$. Figure 8 shows the temperature dependence of ^{1}H NMR spectra of a 1:8 mixture of $(NMe_4)_2[Co\{S\text{-}2,6\text{-}(CF_3CONH)_2C_6H_3\}_4]$ and $(NMe_4)[S\text{-}3,6\text{-}(CF_3CONH)_2C_6H_3]$ in acetonitrile-d_3. The observed sharp signals reveal that the dissociation of ligand is depressed in solution and that the broadening of the signal shown in Figure 7 is caused by the dissociation but not by conformational changes. The signals at 30.6 and −49.3 ppm at −30 °C follow the Curie law to demonstrate the magnetically monomeric structure. These signals are assignable to *m*- and *p*-H of the

(38) Hagen, K. S.; Reynolds, J. G.; Holm, R. H. *J. Am. Chem. Soc.* **1981**, *103*, 4054−4063.
(39) Eaton, D. R.; Josey, A. D.; Benson, R. E. *J. Am. Chem. Soc.* **1967**, *89*, 4040−4050.
(40) Holm, R. H.; Phillips, W. D.; Averill, B. A.; Mayerle, J. J.; Herskovitz, T. *J. Am. Chem. Soc.* **1974**, *96*, 2109−2117.
(41) Reynolds, J. G.; Laskowski, E. J.; Holm, R. H. *J. Am. Chem. Soc.* **1978**, *100*, 5315−5321.

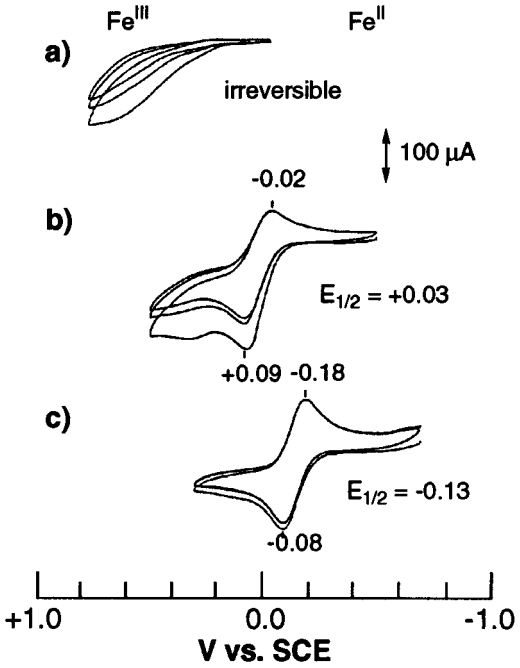

Figure 9. Cyclic voltammograms of a 2.5 mM solution of (a) $(NMe_4)_2[Fe\{S\text{-}2,6\text{-}(CF_3CONH)_2C_6H_3\}_4]$, (b) $(NMe_4)_2[Fe\{S\text{-}2,6\text{-}(CH_3CONH)_2C_6H_3\}_4]$, and (c) $(NMe_4)_2[Fe^{II}(S\text{-}o\text{-}CF_3CONHC_6H_4)_4]$ in acetonitrile. The scan rate is 100 mV/s.

Table 5. Redox Potential (Fe^{III}/Fe^{II}) of Various Thiolato Complexes, $[Fe^{II}(SAr)_4]^{2-}$, in Acetonitrile

SAr	$E_{1/2}$/V vs SCE	$\Delta E_{1/2}$/V[a]
S-2,6-$(CH_3CONH)_2C_6H_3$ (**6a**)	+0.03	+0.56
S-*o*-$CF_3CONHC_6H_4$ (**1a**)	−0.13	+0.40
S-*o*-$CH_3CONHC_6H_4$ (**2a**)	−0.28	+0.25
S-*o*-*t*-$BuCONHC_6H_4$ (**3a**)	−0.29	+0.24
S-*o*-$Ph_3CCONHC_6H_4$ (**4a**)	−0.32	+0.21
S-C_6H_5[b]	−0.53	0
S-*p*-$CH_3CONHC_6H_4$ (**7a**)	−0.57	−0.04

[a] Difference from the redox potential of $[Fe(SPh)_4]^{2-}$. [b] Value from ref 38.

ligand, respectively. A trace of the dimeric species is found, e.g., the signal at ca. −40 ppm. This signal does not follow the Curie law.

Electrochemical Properties. Cyclic voltammograms of $(NMe_4)_2[Fe^{II}\{S\text{-}2,6\text{-}(CF_3CONH)_2C_6H_3\}_4]$ (**5a**), $(NMe_4)_2[Fe^{II}\{S\text{-}2,6\text{-}(CH_3CONH)_2C_6H_3\}_4]$ (**6a**), and $(NMe_4)_2[Fe^{II}(S\text{-}o\text{-}CF_3CONHC_6H_4)_4]$ (**1a**) are shown in Figure 9. The other single NH···S hydrogen-bonded iron(II) complex shows a reversible Fe(III)/Fe(II) redox couple with the similarity to **1a**. In contrast, the double NH···S hydrogen-bonded complex shows a quasi- or irreversible redox couple which reveals an unstable iron(III) oxidation state. The redox potentials for the other related complexes are summarized in Table 5. $\Delta E_{1/2}$ expresses the difference from the redox potential (−0.53 V vs SCE) of the nonsubstituted complex, $(NEt_4)_2[Fe^{II}(SC_6H_5)_4]$.[38] The negative $\Delta E_{1/2}$ value found for **7a** indicates that the inductive effect of acylamino group should not positively shift the redox potential. The observed remarkable positive shift is obviously attributed to the intramolecular NH···S hydrogen bond.

The contribution of NH···S hydrogen bonding to the positive shift of redox potential was proposed for native metalloproteins as early as 1975[3,17] and experimentally supported by the model complexes.[15,20,22,39] The $\Delta E_{1/2}$ value (+0.56 V) for $[Fe^{II}\{S\text{-}2,6\text{-}(CH_3CONH)_2C_6H_3\}_4]^{2-}$ with double NH···S hydrogen bonds is nearly twice as large as that for $[Fe^{II}(S\text{-}o\text{-}CH_3CONHC_6H_4)_4]^{2-}$ with single NH···S hydrogen bonds. These results indicate a linear relationship between the positive shift in redox potential and the number of NH···S hydrogen bond. For **1a** and **5a**, a similar relation is expected. The redox potential of **5a** is estimated at ca. +0.3 V based on the redox potential of **1a** (−0.13 V). The observed trend in $\Delta E_{1/2}$ values among substituents, $CF_3 > CH_3 > t\text{-}Bu > Ph_3C$, is considered due to the electronic effect or variation in the strength of NH···S hydrogen bond as induced by the electronic effect.

The contribution of electrostatic field effect of amide group should be considered here. As we previously reported, *N*-methylation of acylamino group at ortho position decrease dramatically the positive shift of redox potentials, thus the electrostatic effect of the neighboring amide group is considered to be negligible. As Walters *et al*. reported, the hydrogen-bonding *o*-amino group in $[Fe(SC_6H_4NH_2\text{-}2)_4]^{2-}$ does not affect the redox potential. The ^1H NMR signal of NH_2 of the complex in CD_3CN has been reported to be found at 27.9 ppm.[42] On the contrary, amide NH proton in our complex was found at upfield (−6.7 ppm relative to TMS for **3a**) which indicates the presence of directly magnetic interaction through a *covalent* NH···S hydrogen bond as described in the Discussion. These results suggest that the NH_2 group forms a relatively weak NH···S hydrogen bond or electrostatic interaction. On the other hand, the acylamino group forms a strong and covalent NH···S hydrogen bond, which is supported by the restricted amide plane or dipole at the ortho position. We have considered the dipole of amide group directed toward to sulfur is very important to form strong NH···S hydrogen bond.[29]

Recently, Walters *et al*. argued the importance of charge−dipole (C−D) effects on the redox potential of alkanethiolate model complex.[43] The complex, $[Fe^{II}\{SCH_2CON(CH_3)_2\}_4]^{2-}$, having a dipolar neighboring group exhibits a Fe(III)/Fe(II) redox couple at −0.71 V (vs SCE in CH_3CN), which is more positive than the value (−1.10 V) of $[Fe(SCH_2CH_3)_4]^{2-}$. We have previously reported alkanethiolate analogues with NH···S hydrogen bonds, $[Fe^{II}(Z\text{-}\mathbf{cys}\text{-Pro-Leu-}\mathbf{cys}\text{-OMe})_2]^{2-}$ and $[Fe^{II}(Z\text{-}\mathbf{cys}\text{-Pro-Leu-}\mathbf{cys}\text{-Gly-Val-OMe})_2]^{2-}$, which show redox couples at −0.54 and −0.46 V (vs SCE in CH_3CN), respectively.[15] These results suggest that the NH···S hydrogen bond more effectively positively shifts the redox potential than C−D effects.

In the case of arenethiolate complexes, we can find a similar situation. As reported in the literature, $[Mo^{V}O\{S\text{-}2\text{-}CH_3CON(CH_3)C_6H_4\}_4]^-$, $[Mo^{V}O(S\text{-}2\text{-}CH_3CONHC_6H_4)_4]^-$, and $[Mo^{V}O(SC_6H_5)_4]^-$ exhibit the redox couple at −0.71, −0.36, and −0.81 V vs SCE in CH_3CN.[22] The dipolar group, CH_3CONCH_3, at ortho position contributes to the positive shift by only +0.10 V, whereas the combined effect of C−D and NH···S hydrogen bond does so by +0.45 V. The significantly large positive shifts remarkably demonstrate the predominant contribution of the NH···S hydrogen bond to the redox potential.

Oxidation of $(NMe_4)_2[Co^{II}\{S\text{-}2,6\text{-}(CF_3CONH)_2C_6H_3\}_4]$ (5b). As mentioned above the anion $[Fe^{II}\{S\text{-}2,6\text{-}(CF_3CONH)_2C_6H_3\}_4]^{2-}$ is thermally unstable in the oxidized iron(III) state to decompose to unknown species. To investigate the species, chemical one-electron oxidation was performed. Since the iron(II) complex has no characteristic absorption in the visible region, the corresponding cobalt(II) complex was selected and the reaction was monitored by visible spectrum. Figure 10a shows the spectral change on air oxidation of **5b** in acetonitrile. The

(42) Huang, J.; Dewan, J. C.; Walters, M. A. *Inorg. Chim. Acta* **1995**, *228*, 199−206.
(43) Bose, K.; Huang, J.; Haggerty, B. S.; Rheingold, A. L.; Salm, R. J.; Walters, M. A. *Inorg. Chem.* **1997**, *36*, 4596−4599.

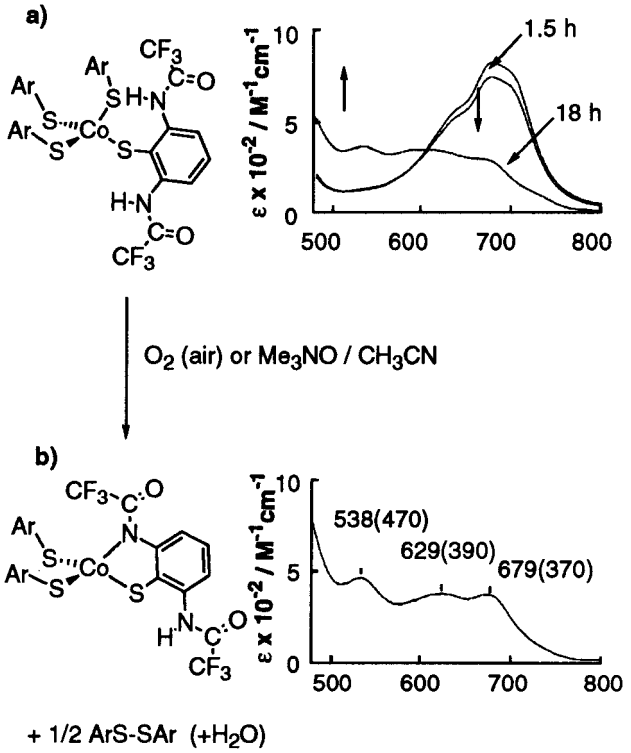

Figure 10. (a) Spectral change in the oxidative reaction of $(NMe_4)_2[Co\{S\text{-}2,6\text{-}(CF_3CONH)_2C_6H_3\}_4]$ (**5b**) and the visible spectrum of $(PPh_4)_2[Co\{S\text{-}2,6\text{-}(CF_3CONH)_2C_6H_3\}_2(S\text{-}2\text{-}CF_3CONH\text{-}6\text{-}CF_3CONC_6H_3)]$ (**9**) in acetonitrile.

resulting product with PPh_4^+ cation, $(PPh_4)_2[Co^{II}\{S\text{-}2,6\text{-}(CF_3CONH)_2C_6H_3\}_2(S\text{-}2\text{-}CF_3CONH\text{-}6\text{-}CF_3CONC_6H_3)]$ (**9**) was isolated in 69% yield whose structure was confirmed by X-ray analysis. The visible spectrum of **9** in acetonitrile shown in Figure 10b indicates a clear agreement with that of the oxidized species in Figure 10a.

The absorption at 600−700 nm of **9** has been considered due to d−d transition. As the absorption at ca. 500−600 nm, which is assignable to ligand field transition with a distorted tetrahedral coordination containing mixed ligands with S_2N_2 donor sets,[44−46] has been reported for the related Co(II) complexes, the absorption at 538 nm is also considered due to d−d transition.

A similar S,N-chelation containing thiolato and deprotonated amide is known for Ni(III).[47] The same deprotonation occurred in the presence of a strong base, e.g. NaH. In the cobalt(II) complex **5b**, the acidity of amide proton was increased by an electron-withdrawing CF_3 group to facilitate the proton loss.

The ^{1}H NMR spectrum of **9** in acetonitrile-d_3 is shown in Figure 11 for comparison with those of **5b** and **1b**. The proton signals at meta and para positions of the S,N-chelate ligand in **9** were found at 32.7, 24.8, and −17.2 ppm. These peaks are relatively sharp because of rigid conformation caused by five-membered ring containing the S,N-chelate. The other peaks of **9** are relatively broad which are similar to those of **5b**. The conformational change of monodentate ligand in **9** is limited by steric congestion as found for **5b**. On the other hand, the complex with free rotating monodentate ligands, e.g., **1b**, shows very sharp signals as shown in Figure 11c.

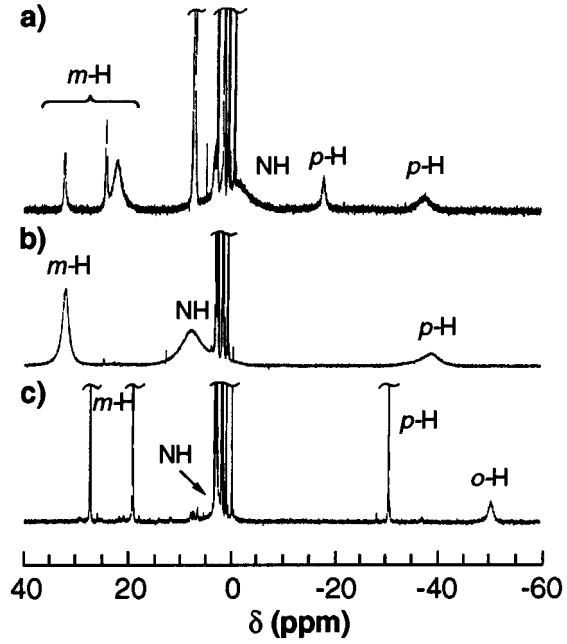

Figure 11. ^{1}H NMR spectra of $(PPh_4)_2[Co\{S\text{-}2,6\text{-}(CF_3CONH)_2C_6H_3\}_2(S\text{-}2\text{-}CF_3CONH\text{-}6\text{-}CF_3CONC_6H_3)]$ (**9**), $(NMe_4)_2[Co\{S\text{-}2,6\text{-}(CF_3CONH)_2C_6H_3\}_4]$ (**5b**), and $(NMe_4)_2[Co(S\text{-}o\text{-}CF_3CONHC_6H_4)_4]$ (**1b**) in acetonitrile-d_3.

Discussion

Short M−S Bonds. The shortening M−S bonds (M = Fe(II) for **3a**, 2.329(8) Å, M = Co(II) for **3b**, 2.296(9) Å; **5b′**, 2.299(14) Å) by NH···S hydrogen bonding can be attributed to antibonding character of the relevant orbitals of the M−S bonds.[16,48] Walters *et al*. have reported a short Co^{II}−S bond (mean 2.302(1) Å) including Co−S_H (S_H = hydrogen-bonded sulfur) and Co−S_N (S_N = non-hydrogen-bonded sulfur). Though the Co−S_N bond (mean 2.294(2) Å) is short, the Co−S_H bond length (mean 2.320(2) Å) is essentially the same as that (2.328(4) Å) of $(Ph_4P)_2[Co^{II}(SC_6H_5)_4]$.[16] The results have been explained by the diminished Co−S antibonding interaction and the partial thioether character of the S_H ligand. In our case, four sulfur ligands are hydrogen-bonded and M−S bonds are shorter than those of non-hydrogen-bonded complexes, $(PPh_4)_2[M(SC_6H_5)_4]$ (M = Fe^{II}, Co^{II}). The same tendency has been found in other complexes having an MS_n (n = 2−4) core without the other coordinated atoms.[16,22,28,29] Such a complex has antibonding M−S character in HOMO. In addition, we could not find any significant difference in the LMCT bands between the hydrogen-bonded and the non-hydrogen-bonded complexes. This result indicates that NH···S hydrogen bonds effectively shorten M−S bonds without drastic changes.

The comparable shortening effect of single and double NH···S hydrogen bonds was found in the present research. The apparent similarity in the M−S bond in **3b** and **5b′** is considered to be caused by the difference of inductive effects between *t*-Bu and CF_3 groups and/or the difference of geometry around the coordinated sulfur atom. The inductive effect of *t*-BuCONH is negligible but CF_3CONH is a weak electron-withdrawing group. An electron-withdrawing group at the thiolato ligand decreases the electron-donating capacity of the sulfur, which will result an elongation of the M−S bond.[31] The single NH···S hydrogen-bonded sulfur was found to have a tetrahedral geometry including one vacant site, one amide proton, the metal,

(44) Corwin, D. T., Jr.; Fikar, R.; Koch, S. A. *Inorg. Chem.* **1987**, *26*, 3080−3082.
(45) Corwin, D. T., Jr.; Gruff, E. S.; Koch, S. A. *J. Chem. Soc., Chem. Commun.* **1987**, 966−967.
(46) Mastropaolo, D.; Thich, J. A.; Potenza, J. A.; Schugar, H. J. *J. Am. Chem. Soc.* **1977**, *99*, 424−429.
(47) Krüger, H.-J.; Holm, R. H. *Inorg. Chem.* **1987**, *26*, 3645−3647.
(48) Harris, S. *Polyhedron* **1989**, *8*, 2843−2882.

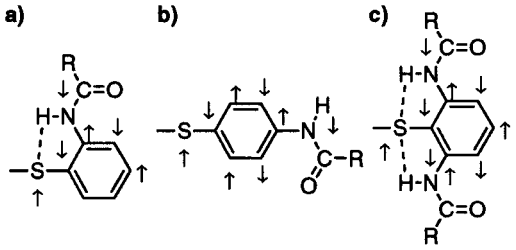

Figure 12. Schematic drawing of spin exchange interactions for (a) *o*- and (b) *p*-(acylamino)-substituted complexes.

and the neighboring carbon atom. On the other hand, the double hydrogen-bonded sulfur has a trigonal bipyramidal geometry formed by two amide protons of both of the ortho positions interacting with the sulfur from the opposite sides. When the two NH···S hydrogen bonds compete each other against the same pπ orbital on sulfur atom, the overall electronic effect must therefore be weakened.

Isotropic Contact Shift through NH···S Hydrogen Bonds. The chemical shift of ^{1}H NMR signal of the NH proton in complexes described above is nicely explained by the NH···S hydrogen bond and paramagnetic influence of the metal. Figure 12 illustrates the magnetic exchange interactions in the *o*- and *p*-acylamino-substituted complexes. The direction of an arrow indicates the sign of an electron spin. The upfield shift of *N*-methyl protons connected with the benzene ring via two σ-bonds in $[Fe_4S_4(SC_6H_4\text{-}p\text{-}NMe_2)_4]^{2-}$ has been explained by the facile spin delocalization from the carbon at para position to the nitrogen without inversion of the sign.[30] The downfield shift of *p*-NH proton in $[Co(S\text{-}p\text{-}t\text{-}BuCONHC_6H_4)_4]^{2-}$ suggests the presence of spin delocalization via hyperconjugation with spin inversion (Figure 12b) which is clearly shown by the downfield shift of *o*-methyl protons in $[Co^{II}(S\text{-}o\text{-}CH_3C_6H_4)_4]^{2-}$. The observed negative sign of the *o*-NH proton shift suggests a delocalization path other than that through the benzene ring. Direct dipolar interaction through space is not a dominant factor since the methyl group and the NH group at ortho position are in similar situations. The orbital sign of spin on sulfur is different from that on nitrogen (Figure 12a). The strong magnetic effect from sulfur through the NH···S hydrogen bond and the relatively weak one from nitrogen through the ordinary π-conjugated system are considered to cause moderately upfield-shifted proton signals. These results strongly support the presence of an intramolecular NH···S hydrogen bond in solution.

The isotropic shift of NH proton in the *doubly* NH···S hydrogen bonded complexes has zero or small positive value as shown in Table 4. In this case, two opposite interactions are present. One is through the phenyl π-system, and the other is through the NH···S hydrogen bond. The former contributes to the upfield shift, and the latter contributes to the downfield shift. The observed small isotropic shift is interpreted by assuming the two interactions to be canceled out. Contrarily, negative isotropic shifts were observed in the *singly* NH···S hydrogen-bonded complexes. In the comparison with the doubly NH···S hydrogen-bonded complexes, these results suggest the presence of rather strong magnetic interaction through the hydrogen bond which is enough to result in an upfield shift even under the opposite effect through the benzene ring.

Structural Change During Oxidative Reaction. A comparison of molecular and crystal structures between **5b′** and **9** is shown in Figure 13. Two of the ligands at the left-hand side (a) in the figure have similar environments. The other two ligands of **5b′** are replaced by one S,N-chelate ligand to limit

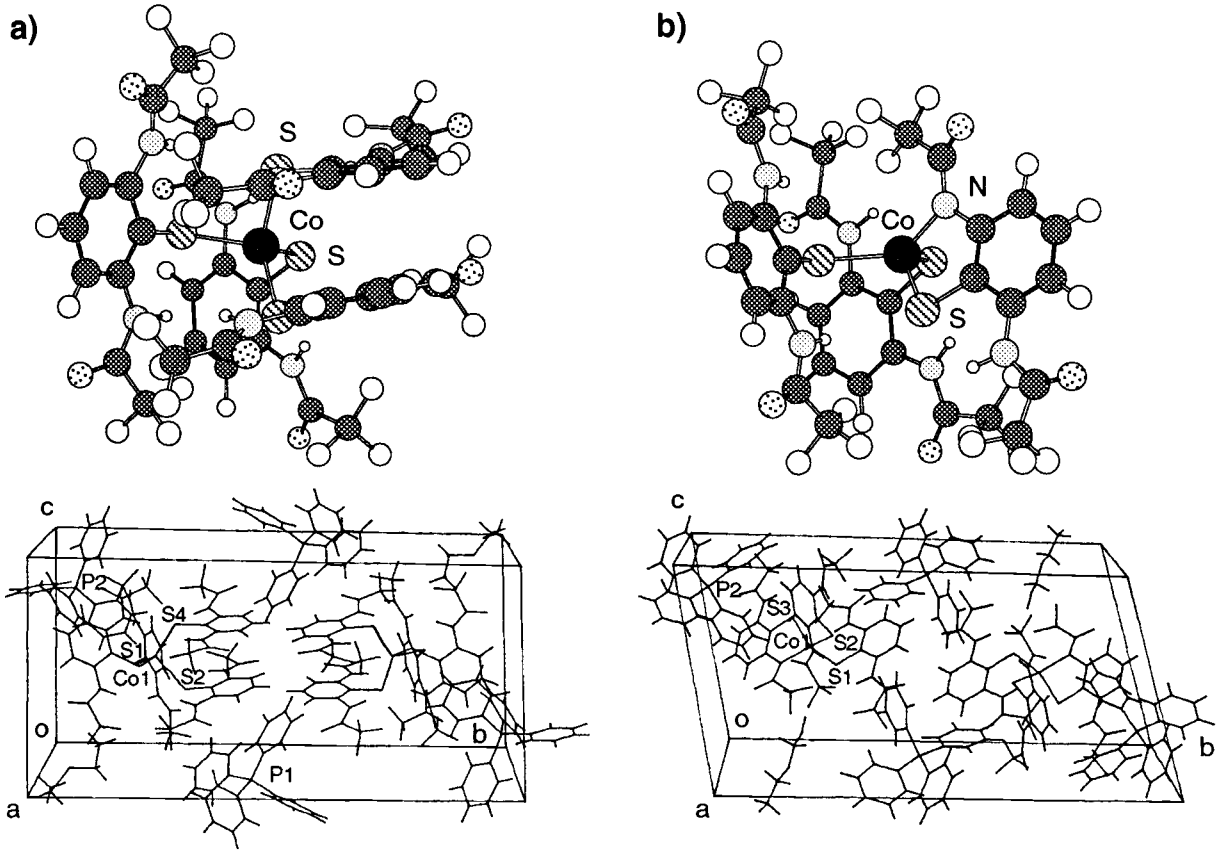

Figure 13. Comparison of molecular structure and crystal packing between (a) $(PPh_4)_2[Co\{S\text{-}2,6\text{-}(CF_3CONH)_2C_6H_3\}_4]\cdot Et_2O$ (**5b′**) and (b) $(PPh_4)_2[Co\{S\text{-}2,6\text{-}(CF_3CONH)_2C_6H_3\}_2(S\text{-}2\text{-}CF_3CONH\text{-}6\text{-}CF_3CONC_6H_3)]\cdot Et_2O$ (**9**).

the steric congestion at the anionic part. The packing of ions of **9** resembles that of **5b′** including the cation and the crystal solvents (Figure 13). The result suggests that the structural change from **5b′** to **9** during oxidative reaction occurred easily without any steric barrier. In this reaction the oxidation at cobalt(II) has not been observed, and thus an electron is considered to be transferred to the metal from each of the dissociated thiolate ligands to form diaryl disulfide through radical recombination. One of the amide protons of **5b′** was deprotonated to give water during O_2^- or amine *N*-oxide oxidation. When one electron oxidant lacking ability of oxygen atom transfer, e.g. $[FeCp_2]^+$ or TCNQ (7,7,8,8-tetracyanoquinodimethane), was used, the reaction did not give complex **9** but only unidentified species.

The electron-withdrawing group, CF_3, presumably increases the acidity of amide NH proton to ease the deprotonation at NH. The electrochemical oxidation of $[Fe^{II}\{S\text{-}2,6\text{-}(CF_3CONH)_2C_6H_3\}_4]^{2-}$ is considered to proceed in a similar way but gave unidentified species in such an oxygen-free system without formation of water from proton of NH. Consequently, an irreversible Fe^{III}/Fe^{II} redox couple was observed for $(NMe_4)_2[Fe^{II}\{S\text{-}2,6\text{-}(CF_3CONH)_2C_6H_3\}_4]$ (**5a**) as mentioned above (Figure 9).

Biological Relevances of NH···S Hydrogen Bonding. Control of redox potential is very important in biological systems, especially in electron transfer proteins. The effects of NH···S hydrogen bond have already been discussed for bacterial ferredoxins with [4Fe-4S] clusters containing four FeS^*_3S (S* = inorganic sulfur) iron cores,[3,8,49] including the high-potential iron−sulfur proteins (HiPIPs) which function in the redox cycle between $[Fe_4S_4(Cys)_4]^{1-/2-}$ that ranges from +50 to +450 mV.[8,50] Since [4Fe-4S] cores of both ferredoxins and HiPIPs resemble each other in Raman spectroscopy,[8] the large difference in the redox behavior has been ascribed to the hydrophobicity around the [4Fe-4S] core and to the number of NH···S hydrogen bonds through the investigation based on X-ray analysis or theoretical approach.[3,17,18] In native ferredoxin, eight NH···S hydrogen bonds including NH···S* (S* = bridged inorganic sulfur) are found, and in HiPIP, six NH···S hydrogen bonds including two NH···S* are found. The larger number of NH···S hydrogen bond results in the appearance of a more positively shifted redox potential. The shift value of the redox potential per one NH···S hydrogen bond has been estimated to range from 0.072 V/NH to 0.080 V/NH.[17] In our case, the complex **3a** shows more positive redox couple than that of a non-hydrogen-bonded complex, $(NEt_4)_2[Fe(SC_6H_5)_4]$, by +0.24 V (+0.06 V/NH).

Rubredoxins are known to have two parts of chelating peptide segments containing invariant amino acid sequences, Cys(1)-X_1-X_2-Cys(2)-Gly-X_3 (X_2, X_3 = amino acids, X_3 = Val, Ala), which include three intramolecular NH···S hydrogen bonds (X_2 → Cys(1), Cys(2) → Cys(1), and X_3 → Cys(2)).[51] These sequences support the preferable location of the amide NH groups for NH···S hydrogen bonds and are essential for controlling the redox potentials. Two of the three hydrogen bonds, X_2 → Cys(1) and Cys(2) → Cys(1), are buried inside of Cys(1)-X_1-X_2-Cys(2) chelation and shielded from solvent. The fixed amide NH of the ligand in this study at the 2- or 2,6-positions is a satisfactory model to reconstruct the situation of the amide group in the conserved peptide sequence and successfully realized intramolecular NH···S hydrogen bond observed in many of the biological systems.

Conclusion

Novel simple rubredoxin model iron(II) complexes and the related cobalt(II) derivatives with single and double NH···S hydrogen bonds were synthesized and characterized. The presence of NH···S hydrogen bond was established by X-ray analysis, and the relative strength was inferred from ^{1}H NMR and IR spectra. These model complexes are now indicated to have the contribution of the NH···S hydrogen bond to the positive shift of redox potential in an additivity relationship. In the ^{1}H NMR, the isotropic contact shift of the NH protons through intramolecular hydrogen bond was interpreted to support the above conclusion.

Acknowledgment. Support of this work by a Grant-in-Aid for Specially Promoted Research (06101004) from the Ministry of Education, Science and Culture of Japan is gratefully acknowledged.

Supporting Information Available: Listings of final positional and thermal parameters,and intramolecular bond angles and distances for **3a**, **3b**, **5b′**, and **9** (29 pages). X-ray crystallographic files, in CIF format, for complexes, **3a**, **3b**, **5b′**, and **9** are available on the Internet only. Ordering or access information is given on any current masthead page.

IC970640B

(49) Armstrong, F. A.; George, S. J.; Thomson, A. J.; Yates, M. G. *FEBS Lett.* **1988**, *234*, 107−110.

(50) Meyer, T. E.; Przysiecki, C. T.; Watkins, J. A.; Bhattacharyya, A.; Simondsen, R. P.; Cusanovich, M. A.; Tollin, G. *Proc. Natl. Acad. Sci. U.S.A.* **1983**, *80*, 6740−6744.

(51) Frey, M.; Sieker, L.; Payan, F.; Haser, R.; Bruschi, M.; Pepe, G.; LeGall, J. *J. Mol. Biol.* **1987**, *197*, 525−541.